Raman and x-ray diffraction investigations on $BaMoO_4$ under high pressures

2006 J. Phys.: Condens. Matter 18 3917

(http://iopscience.iop.org/0953-8984/18/16/002)

INSTITUTE OF PHYSICS PUBLISHING JOURNAL OF PHYSICS: CONDENSED MATTER

J. Phys.: Condens. Matter **18** (2006) 3917–3929 doi:10.1088/0953-8984/18/16/002

Raman and x-ray diffraction investigations on $BaMoO_4$ under high pressures

Vinod Panchal, Nandini Garg and Surinder M Sharma[1]

Synchrotron Radiation Section, Bhabha Atomic Research Centre, Mumbai 400085, India

E-mail: smsharma@magnum.barc.ernet.in

Received 3 January 2006
Published 3 April 2006
Online at stacks.iop.org/JPhysCM/18/3917

Abstract

X-ray diffraction and Raman scattering studies on the scheelite structured barium molybdate show that, at ∼5.8 GPa, it undergoes a first order phase transition to the fergusonite structure ($I2/a$, $Z = 4$)—as also observed in iso-structural barium tungstate. At still higher pressures, barium molybdate transforms to another phase between ∼7.2 and 9.5 GPa. On release of pressure from 15.8 GPa, the initial phase is recovered, implying that the observed structural modifications are reversible.

1. Introduction

Scheelite structured alkaline earth tungstates and molybdates are technologically important materials as these are used as scintillators [1], laser host materials [2] or cryogenic detectors for dark matter [3]. These tungstates are also being considered for Raman lasers [4]. In these scheelite structured compounds (space group $I4_1/a$, $Z = 4$), oxygen atoms form a distorted simple cubic arrangement, while the two cations in this structure have fourfold and eightfold coordination with the oxygen atoms. To understand the structural stability under different thermodynamic conditions, many scheelite compounds have been extensively studied [5–12]. In particular, under high pressures, the scheelite structured alkaline earth molybdates and tungstates show several phase transitions [7–12]. Based on the packing efficiency considerations, some of the earlier studies on these compounds suggested that wolframite [8, 13] may be a preferred high pressure structure [14]. However, recent high pressure investigations have shown that these compounds may transform to any of the competing monoclinic structures, such as wolframite [8, 13], fergusonite [7, 9, 15, 16], or $HgMoO_4$ [12]. For example, barium tungstate [9] has been shown to transform to the fergusonite structure at ∼7 GPa. Even $CaWO_4$, which was viewed as a strong candidate for the wolframite structure at high pressures [17], has been shown to transform to the fergusonite phase at 11.2 GPa [18]. Recent XANES and x-ray diffraction (XRD) studies on $SrWO_4$ [19, 20]

[1] Author to whom any correspondence should be addressed.

and XRD studies on $CaMoO_4$ [21] have shown that they also belong to the same category, i.e. they too transform to the fergusonite phase at 9.9 GPa. Apart from these crystal to crystal phase transitions, Grzechnik *et al* [22] have shown that some of the scheelite fluorides undergo a pressure induced amorphization, which is driven by the chemical decomposition as also observed in several other compounds [23].

Though the first high pressure phase transition in these scheelite compounds appears to be well studied, the second high pressure phase has not yet been determined conclusively. For $YliF_4$, the electronic structure calculations by Li *et al* [24], on several competing structures, such as $BaWO_4$-II, $LaTaO_4$, $BaMnO_4$ and wolframite, have shown that the post-fergusonite phase may be similar to wolframite. In contrast, the *ab initio* total energy calculations of Errandonea *et al* [19] show that for $CaWO_4$ and $SrWO_4$, an orthorhombic $Cmca$ phase (which has not been so far observed experimentally in these compounds) is more stable than the fergusonite phase beyond 29 and 21 GPa respectively. They also indicate that $LaTaO_4$ structure may be in close competition with the $Cmca$ phase for the second high pressure phase for $SrWO_4$. There is yet another experimental study which found this transformation to be irreversible and is ascribed to an onset of decomposition in $SrWO_4$ beyond 15 GPa [20].

Recently, the high pressure behaviour of another member of this group, $BaMoO_4$, has been investigated with the help of Raman studies up to 8 GPa and it indicates a phase transition at ∼5.8 GPa [25]. To gain further understanding of the structural chemistry of this family, and also to determine the structure of the high pressure phase in $BaMoO_4$, we have carried out synchrotron based angle dispersive x-ray diffraction experiments. In addition, Raman measurements were also extended up to ∼13 GPa. We present here our results of these investigations and compare these with the results of other closely related compounds.

2. Experimental details

High pressure Raman and x-ray diffraction studies were carried out on the powder samples of barium molybdate (Aldrich chemicals (purity 99.9%)). Raman spectra were recorded using a CCD based single stage spectrograph employing a super-notch filter. The 514.5 nm line of the argon ion laser was used as an excitation source. The Raman signal was collected in the back-scattering geometry, with the laser beam incident upon the sample at an angle of ∼45° with respect to the axis of collection optics. Several modes lying in between 250 and 1000 cm^{-1} were recorded as a function of pressure. Reasonably good quality Raman data could be obtained with typical collection times of ∼100 s.

Angle dispersive x-ray diffraction measurements were carried out at the XRD1 beamline at the Elletra synchrotron source using monochromatic x-rays of wavelength 0.6967 Å (calibrated using a LaB_6 NIST standard). The x-rays were collimated to ∼100 μm and the two dimensional diffraction rings, collected on a MAR 345 imaging plate, were converted to one dimensional diffraction profiles using the FIT2D software [26]. The cell parameters were determined using Le Bail analysis incorporated in the GSAS software [27]. Using the same software, Rietveld analysis was also carried out for the initial scheelite and the first high pressure phase.

For both the studies, the powder sample of $BaMoO_4$ was loaded in a hole of ∼130 μm diameter of a pre-indented (80 μm) tungsten gasket, which was mounted in a Mao–Bell type of diamond anvil cell. 4:1 methanol–ethanol mixture was used as a pressure transmitting medium. In the Raman experiments ruby R-lines were used for the pressure calibration [28], whereas for the x-ray diffraction experiments gold was used as a pressure marker. The pressure on the sample in the x-ray diffraction experiments was deduced using the equation of state of gold as given in [29].

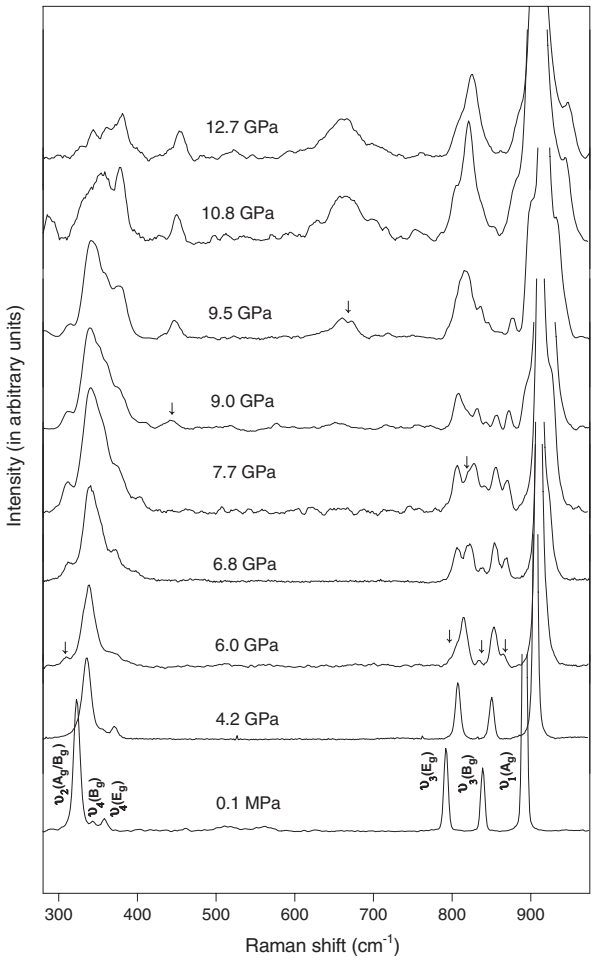

Figure 1. Background subtracted Raman spectra of $BaMoO_4$ at various pressures. The arrows indicate the new Raman modes.

3. Results and discussion

3.1. Raman scattering

At ambient conditions, $BaMoO_4$ exists in the scheelite structure (space group $I4_1/a$ and point group C_{4h}^6) with two formula units per primitive cell (four formula units in the conventional body centred tetragonal unit cell). The group theoretical analysis predicts that the optical phonons belong to the following irreducible representations of the point group C_{4h}^6, $3A_g+5B_g+5E_g+4A_u+3B_u+4E_u$. Of these, the A_g, B_g, and E_g modes are Raman active and A_u, B_u, and E_u are infrared active. Raman active internal modes due to MoO_4 tetrahedra are identified as ν_1 (A_g), ν_3 (B_g and E_g) (stretching modes), and ν_2 (A_g and B_g), ν_4 (B_g and E_g) (bending modes) [12]. At ambient conditions, we have retained the assignments given by Jayaraman *et al* [12], which were based on the earlier work of Liegeois-Duyckaerts and Tarte [30].

Raman spectra of $BaMoO_4$ at a few representative pressures are shown in figure 1. The observed Raman modes above 250 cm^{-1} are known to be the internal modes of MoO_4

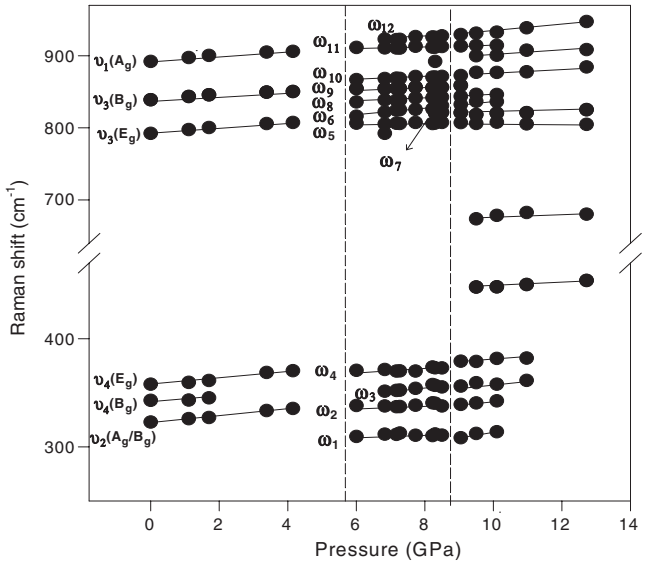

Figure 2. Pressure dependence of Raman modes of barium molybdate. ν_1–ν_4 represent the Raman modes of the scheelite phase and ω_1 to ω_{12} are the Raman modes of the new high pressure phase (fergusonite). The solid lines are drawn as a guide to the eye. The vertical dashed lines indicate the pressures beyond which the phase transitions to the new phases were observed.

tetrahedra. Figure 2 shows that, in the scheelite phase, all the observed modes display a gradual stiffening with pressure. At ∼6 GPa, some new modes appear at ∼309 cm^{-1} (ω_1), 806 cm^{-1} (ω_5), 835 cm^{-1} (ω_8), and 866 cm^{-1} (ω_{10}). On further increase of pressure to 6.8 GPa, several of these changes in the Raman spectra became more clearly visible. Moreover, around this pressure, the accidental degeneracy of $\nu_2(A_g + B_g)$ modes was removed, as has also been observed in iso-structural $SrWO_4$ and $CaWO_4$ [31]. In addition, Raman modes show a change in slope ($d\omega/dP$) around this pressure. These observed changes in the Raman spectra indicate a phase transition, probably to a lower symmetry phase (phase II). These results, before and across ∼6 GPa, are similar to those obtained recently by Christofilos *et al* [25]. It is also interesting to note that the pressure of this transformation is quite close to the transformation pressure of ∼7 GPa observed in iso-structural $BaWO_4$ [9].

The slope ($d\omega_i/dp$) and the corresponding mode-Grüneisen parameters of various Raman modes are listed in table 1. For mode-Grüneisen parameters, we have used the bulk moduli obtained from our x-ray diffraction studies (presented in the next section). The slopes of most of the internal modes in the scheelite phase have comparable values. Comparison of the corresponding Grüneisen parameters for $BaMoO_4$, $BaWO_4$, and $CaMoO_4$ shows that these are also qualitatively similar. These results suggest that the pressure induced changes in the force constants of these scheelite structured compounds are similar, particularly for the higher frequency modes.

On increasing the pressure further, at ∼7.7 GPa we observed broadening of several Raman peaks along with the appearance of a new mode at 820 cm^{-1} (marked with an arrow in figure 1). At still higher pressures, another mode also starts developing at 450 cm^{-1} accompanied by a change of slope of the Raman modes at ∼9 GPa. At ∼9.5 GPa an additional new Raman mode was also observed at ∼675 cm^{-1}. In addition, the intensity of the mode at 806 cm^{-1} also increased significantly. No more changes were observed in the Raman spectra till ∼12.7 GPa.

Table 1. Observed Raman frequencies, pressure dependence and mode-Gruneisen parameter ($\gamma_{i=} - \mathrm{d}\ln\omega_i/\mathrm{d}\ln V = (B_0/\omega_i)(\mathrm{d}\omega_i/\mathrm{d}p)$ for the scheelite phase of $BaMoO_4$. (B_0 is the bulk modulus and ω_i is the phonon frequency.) Column 4 also lists the values of Grüneisen parameters for the modes of the same symmetry in $BaWO_4$ and $CaMoO_4$. For $BaWO_4$, Grüneisen parameter has been scaled to the experimental value of the bulk modulus (57 GPa [9]) compared to the value (40 GPa) used by Jayaraman *et al* [12]. The observed Raman active modes and their pressure dependence in the fergusonite phase are also listed. (The values of $\omega_3, \omega_7, \omega_{12}$ have been obtained by extrapolating to 6.0 GPa.)

Scheelite phase					Fergusonite phase		
ω (cm^{-1})	$d\omega/dP$ (cm^{-1} GPa^{-1})	γ_i	γ_i $BaWO_4$ ($CaMoO_4$)	Mode assignment	Raman mode	ω_R at 6 GPa (cm^{-1})	$d\omega/dP$ (cm^{-1} GPa^{-1})
322	2.54	0.44	0.54	$A_g/B_g(\nu_2)$	$\omega1$	309	−1.34
			(0.82)		$\omega2$	338	0.58
343	3.05	0.50	0.33	$B_g(\nu_4)$	$\omega3$	351	2.89
			(0.81)		$\omega4$	370	4.54
358	3.27	0.51	—	$E_g(\nu_4)$	$\omega5$	806	0.55
			(0.98)		$\omega6$	816	5.08
792	4.25	0.30	0.23	E_g (ν_3)	$\omega7$	820	0.93
			(0.32)		$\omega8$	835	2.49
839	2.87	0.19	0.16	$B_g(\nu_3)$	$\omega9$	854	1.01
			(0.21)		$\omega10$	866	1.77
892	3.66	0.23	0.17	$A_g(\nu_1)$	$\omega11$	911	0.71
			(0.20)		$\omega12$	923	2.84

These observed changes in the Raman spectra may not be attributable to the non-hydrostatic pressures arising due to the freezing of the liquid pressure medium, as even in our x-ray diffraction studies (to be discussed in the next section) we observed new diffraction peaks around this pressure. Due to the continuation of all the modes from 7.7 to 9.5 GPa and from the emergence of new modes, we conclude that another phase change which is initiated between 7 and 7.7 GPa is completed by ∼9.5 GPa. Moreover, the appearance of a new mode at 675 cm^{-1}, i.e. in the gap of ∼400–780 cm^{-1} of the scheelite and the first high pressure phase (phase II), suggests that the structure of the new phase may be quite different from the preceding phases. It should be noted that a similar second phase transition was also observed in several other scheelite structured compounds like $YLiF_4$ and $BaWO_4$ at 17, and 14 GPa respectively [7, 9]. Recent first principles total energy calculations by Errandonea *et al* [19] also predicted that $CaWO_4$ may transform to a second high pressure phase at ∼29 GPa and $SrWO_4$ may do so at ∼21 GPa. Their results suggest that in the new structure ($Cmca$) the counter-cation (Ca and Sr) would be coordinated to six oxygen atoms. Such a coordination change in $BaMoO_4$ may be consistent with the appearance of the new Raman modes at 675 cm^{-1}. We also note that Grzechnik *et al* [20] have reported that in $SrWO_4$ the fergusonite phase decomposes into its constituent oxides WO_3 and SrO, WO_3 having a sixfold coordination with oxygen. Though in principle the appearance of the mode at 675 cm^{-1} may also indicate a similar possibility in $BaMoO_4$, the x-ray diffraction results given below show no identifiable abundance of the decomposition products.

3.2. X-ray diffraction

To determine the structure of the new phases observed in the Raman spectra, x-ray diffraction studies were carried out. X-ray diffraction profiles of barium molybdate at a few pressures are

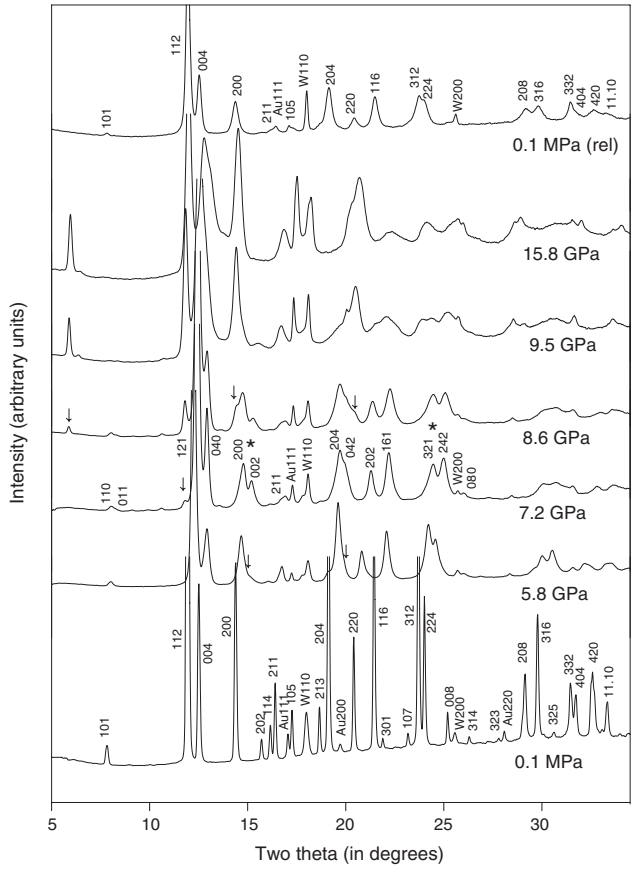

Figure 3. X-ray powder diffraction patterns of $BaMoO_4$ at various pressures. Au (*hkl*) and W (*hkl*) are the diffraction peaks from gold and tungsten respectively. The initial and first high pressure phase have been indexed with the scheelite and the fergusonite structure respectively.

shown in figure 3. The diffraction peaks of gold and tungsten are marked as Au (*hkl*) and W (*hkl*) respectively. Before we present the analysis, we will list the observed changes in the diffraction pattern under pressure. The diffraction pattern evolves smoothly up to 5 GPa. At ∼5.8 GPa most of the diffraction peaks showed broadening and weak shoulders developed at $2\theta \sim 15.2°$ and 20° (marked with arrows in figure 3). However, at 5.8 GPa, the diffraction pattern is still indexable in the scheelite phase. At ∼7.2 GPa, apart from the broadening of the diffraction peaks, several new diffraction peaks were also observed and the shoulders that appeared at 5.8 GPa also developed into clearly identifiable diffraction peaks. The splitting of the (200) and intensity redistribution of (312) and (224) diffraction peaks (marked with * in figure 3) is also easily identifiable. These results indicate that beyond 5.8 GPa $BaMoO_4$ transforms to phase II as also implied by the changes in the Raman spectra at ∼6 GPa. On further increase of pressure to ∼8.6 GPa, a new diffraction peak appeared at $\sim 2\theta = 5.8°$ and weak shoulders started developing at $2\theta \sim 14.4°$ and 20.4°. Apart from these changes the rest of the diffraction pattern was similar to that of phase II. At 9.5 GPa the intensity of the diffraction peak at $\sim 2\theta = 5.8°$ further increased and this is also accompanied by more changes in the diffraction pattern. Detailed analysis of the evolution of the diffraction pattern (given in the next paragraph) shows that phase II begins to transform to another phase at ∼7.2 GPa

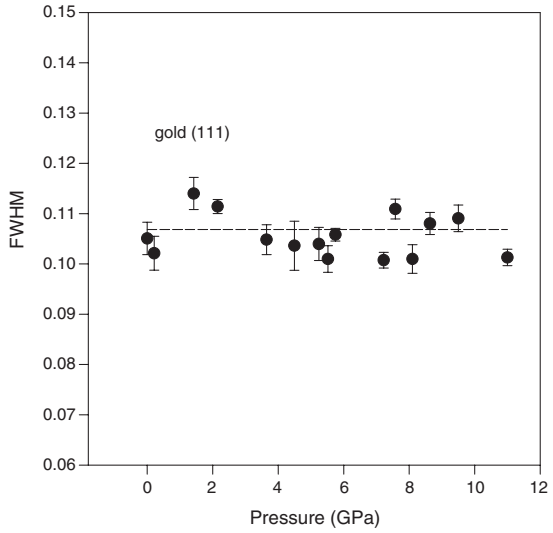

Figure 4. The pressure dependence of the FWHM of the (111) diffraction peak of gold, which was used as an internal pressure marker in the x-ray diffraction study.

and this transformation is completed by ∼9.5 GPa. The appearance of a diffraction peak at lower 2θ value indicates unit cell enlargement. This phase continues to exist up to the highest pressure of this study, i.e. 15.8 GPa. The sample environment across this transition was quasi-hydrostatic, as can be seen from the plot of the full width at half maximum in figure 4 of the gold (111) diffraction peak.

On release of pressure, the initial phase is fully recovered as observed in other molybdates and tungstates of this family of compounds [9, 10, 32]. However, as shown in figure 3, the diffraction peaks retain some broadening on release of pressure. This may be due to the residual strains in the polycrystalline samples, as this pattern was recorded immediately after release of pressure from 15.8 GPa. The non-observability of the diffraction peaks of the probable decomposition products and the reversibility of the high pressure phase to the scheelite phase on release of pressure imply that $BaMoO_4$ does not decompose significantly into the component oxides at high pressures, unlike what was observed in a recent high pressure study on $SrWO_4$ [20].

At ambient conditions 26 diffraction peaks of the scheelite phase (phase I) are identifiable. Some of the *hkl* indices for the scheelite phase are marked in figure 3. The lattice parameters of the scheelite phase are found to be $a = 5.5800 \pm 0.0004$ Å and $c = 12.820 \pm 0.002$ Å, which are in very good agreement with the published lattice parameters, namely, $a = 5.58$ Å and $c = 12.82$ Å (ICDD card no 29-0193). Rietveld analysis of the diffraction pattern at ambient conditions shows that the atomic positional parameters (shown in table 2) are in good agreement with the earlier reported values.

The Rietveld analysis of the diffraction pattern at ∼5.8 GPa shows that it can still be fitted in the scheelite phase excluding the two weak shoulders. The presence of these two shoulders indicates that transformation to a new structure was initiated at this pressure. However, the analysis of the diffraction pattern at 7.2 GPa indicates that a phase transformation has taken place, probably to a lower symmetry phase (phase II), in agreement with our Raman results. Le Bail analysis of the diffraction pattern at this pressure showed that it can be fitted to a monoclinic space group with $I2/a$ symmetry (i.e. fergusonite—a distorted scheelite structure)

Table 2. (a) Structural parameters for scheelite $BaMoO_4$ at ambient condition. The space group is $I4_1/a$ ($Z = 4$) and the lattice parameters are $a = 5.5800 \pm 0.0004$ Å, $c = 12.820 \pm 0.002$ Å. (b) Structural parameter for fergusonite $BaMoO_4$ phase at 7.2 GPa. The space group is $I2/a$ ($Z = 4$) and the lattice parameters are $a = 5.425 \pm 0.001$ Å, $b = 12.397 \pm 0.003$ Å, $c = 5.260 \pm 0.001$ Å and $\beta = 89.530° \pm 0.001$. (Estimated standard deviations are given in parenthesis.)

(a)				
Atom	Site	x	y	z
Ba	4b	0.0000	0.0000	0.5000
Mo	4a	0.0000	0.0000	0.0000
O	16f	0.2435(9)	0.1146(8)	0.0751(1)
		Bond lengths (Å)		
Mo–O	1.778 (20)	Ba–O1	2.745 (18)	
		Ba–O2	2.724 (18)	
(b)				
Atom	Site	x	y	z
Ba	4e	0.2500	0.6242(4)	0.0000
Mo	4e	0.2500	0.1280(8)	0.0000
O	8f	0.8584(2)	0.9451(6)	0.2490(2)
O	8f	0.4973(1)	0.1998(1)	0.8836(1)
		Bond lengths (Å)		
Mo–O1	1.699(5)	Ba–O1	2.644(12)	
Mo–O2	1.713(6)	Ba-O2	2.646(12)	
		Ba-O3	2.598(12)	
		Ba-O4	2.639(12)	

except for a weak diffraction peak at $2\theta \sim 11.8°$.[2] For Rietveld analysis of phase II, the initial coordinates were obtained by transforming the coordinates of the scheelite phase at 5.8 GPa to the coordinates of the $I2/a$ space group using the group–subgroup relations as incorporated in the Powdercell software [33]. A typical fit to the data at this pressure is shown in figure 5 and the parameters of goodness of fit are $R_{wp} = 8.7\%$, $R_p = 6.6\%$. Therefore, it may be reasonable to accept that this phase has a fergusonite structure, similar to the high pressure phase observed in $BaWO_4$, $CaWO_4$, $SrWO_4$, and $CaMoO_4$ [9, 18, 19, 21]. The structure of this phase is related to the initial scheelite phase through a correlated displacive atomic motion. For this, all the atoms of alternate layers of the scheelite structure need to shift in opposite directions along the c-axis, as shown by the arrows in figure 6. The a-axis of the monoclinic cell ($\mathbf{a}_m$) lies along the a-axis of the tetragonal cell ($\mathbf{a}_t$), but $\mathbf{b}_m$ lies along $\mathbf{c}_t$ and $\mathbf{c}_m$ is along the $\mathbf{b}_t$ [9].

The cell constants and the coordinates of the new phase have been listed in table 2. The Mo–O and Ba–O bond distances for the tetragonal and monoclinic phases are also given in this table. Deduced Mo–O and Ba–O bond lengths in the monoclinic phase imply that MoO_4 tetrahedra as well as BaO_8 octahedra are distorted in this phase. Moreover, reduced bond lengths at ~7 GPa imply that in barium molybdate the phase transformation to the denser phase affects both—the tetrahedra as well as octahedra, unlike in the scheelite phase as discussed later.

The variations of the cell constants and volume (V/V_0) with pressure are shown in figures 7(a), (b), (c), and (d) respectively. Across the phase change to the fergusonite phase,

[2] The intensity of this weak diffraction peak, first observed at 7.2 GPa, increases with pressure and it is one of the strongest peaks of the next high pressure phase. This, along with the observation of subtle changes in the Raman spectra at ~7.7 GPa, suggests the onset of the second high pressure phase transition is at somewhat lower pressures, i.e. ~7.2 GPa.

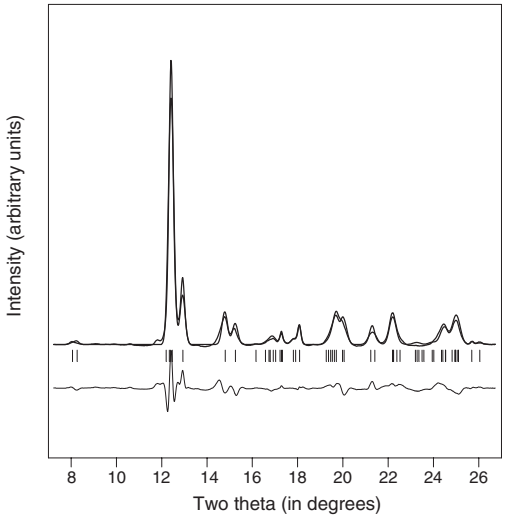

Figure 5. Observed, calculated, and difference x-ray diffraction patterns for the fergusonite ($I2/a$, $Z = 4$) phase of $BaMoO_4$ at 7.2 GPa. Bars indicate the expected positions of diffraction peaks.

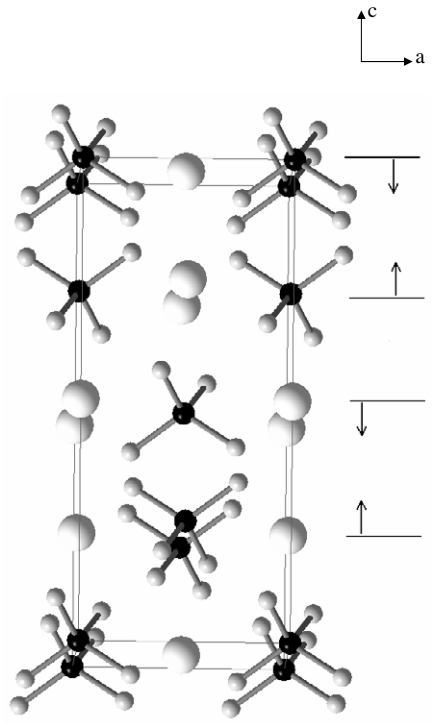

Figure 6. The scheelite structure of $BaMoO_4$. For the structural change from scheelite to the fergusonite phase, the arrows indicate the direction of displacement of all the atoms in the alternate layers.

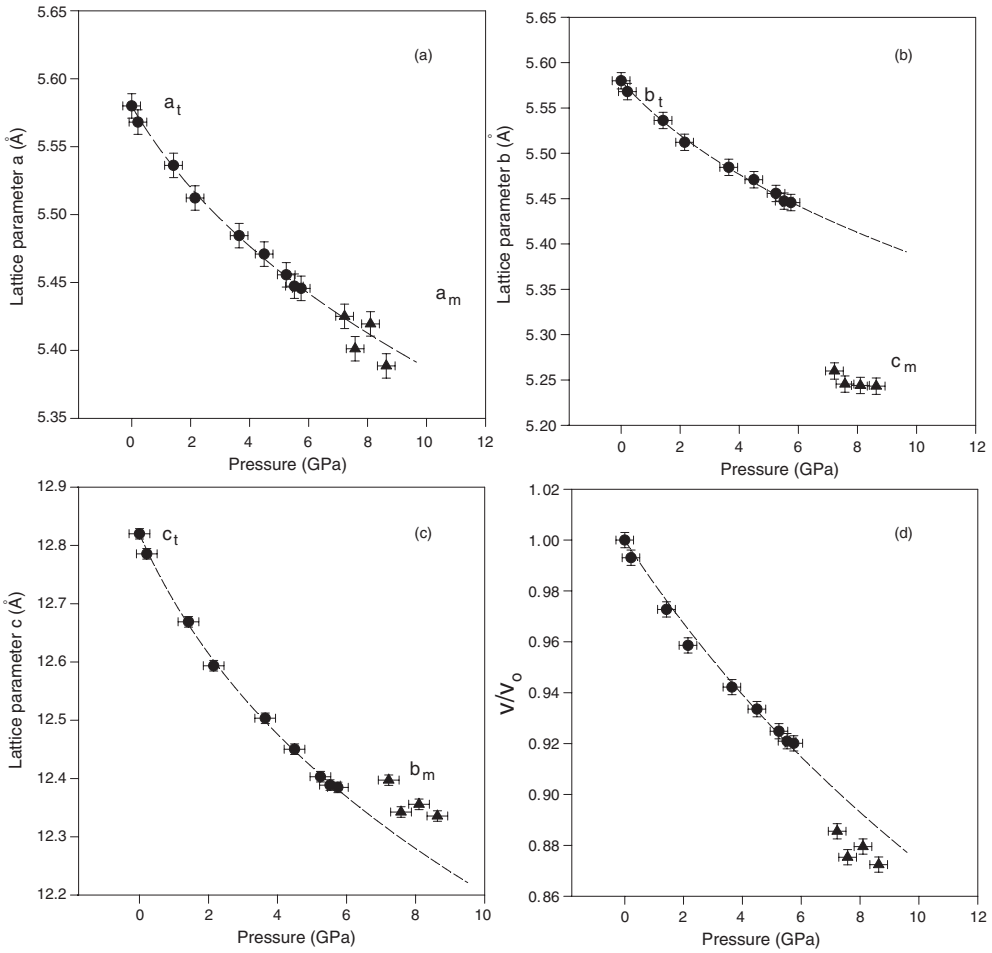

Figure 7. Pressure dependence of lattice parameters and V/V_0 for the scheelite and the fergusonite phases of $BaMoO_4$. The dashed lines in (a), (b), and (c) are the quadratic fits to the respective lattice parameters up to 9.5 GPa. The subscripts t and m represent the tetragonal (scheelite) and monoclinic (fergusonite) phases respectively. (a) Lattice parameter **a** for the scheelite phase (●) and for the fergusonite phase (▲). (b) Lattice parameter **b** for the scheelite phase (●) and **c** for the fergusonite phase (▲). (c) Lattice parameter **c** for the scheelite phase (●) and **b** for the fergusonite phase (▲). (d) V/V_0 of $BaMoO_4$ (●) for the scheelite phase and (▲) for the fergusonite phase. In this figure V_0 refers to that of the scheelite phase at ambient conditions. The dashed line shows the fit to Birch–Murnaghan equation of state in the scheelite phase.

the lattice parameters a and b differ from those of the scheelite structure only marginally. However, we observe a decrease of 3.4% in the $\mathbf{b}_t$. It is also seen that the $\mathbf{c}_t/\mathbf{a}_t$ ratio of the tetragonal phase decreases and the $\mathbf{b}_m/\mathbf{c}_m$ and $\mathbf{b}_m/\mathbf{a}_m$ ratios of the fergusonite phase increase and decrease respectively, a feature similar to the observations in barium tungstate [9] and calcium tungstate [18]. It should also be noted that in the scheelite fluorites and rare earth niobates and tantalates the c/a ratio of the scheelite phase is known to increase but the respective ratios of the unit cell constants in the fergusonite phase have similar trends as alkaline tungstates and molybdates. These differences may be due to the trivalent cation of the MX_4 (M = Y, Ta, Nb, Lu) tetrahedra in these compounds.

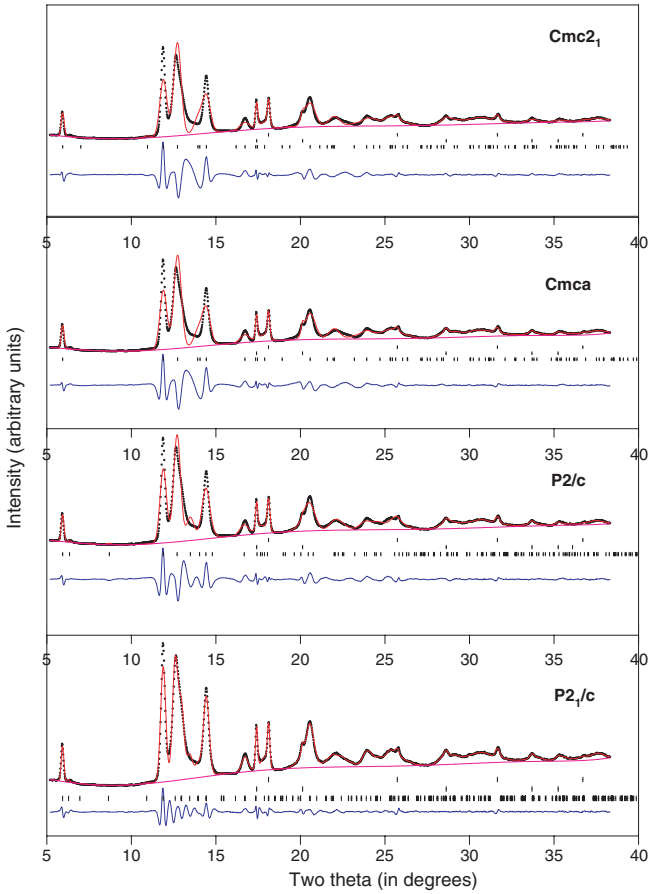

Figure 8. Observed, calculated and difference x-ray diffraction patterns for the second high pressure phase of $BaMoO_4$ at 11 GPa. Bars indicate the expected positions of the diffraction peaks.
(This figure is in colour only in the electronic version)

Figure 7(d) shows that V/V_0 drops by ∼3.6% across the phase transition to the fergusonite phase, which is comparable to that observed in barium tungstate. In other scheelites like $YLiF_4$, even though the experimental results show a negligible volume change across the scheelite to fergusonite phase transition, electronic energy calculations suggest a volume collapse of ∼0.5% across the phase transition. In $SrWO_4$ and $CaWO_4$, also no detectable volume discontinuity was observable at the scheelite to fergusonite phase transition [19, 20].

The P–V data of barium molybdate in the tetragonal phase, fitted to the second order Birch–Murnaghan equation of state, gives the bulk modulus to be 56 GPa with $K' = 4$. Corresponding values for $BaWO_4$ are 57 GPa $K' = 3.5$. These results indicate that in the scheelite phase the compression of these compounds is similar. These results are also consistent with an empirical correlation between the compressibility of the scheelite oxides and the cation–oxygen bond distances [15, 19]. According to this empirical relationship, the polyhedral bulk modulus is approximately given as K_p (in GPa) $= 610\ Z_i/d^3$, where Z_i is the cationic formal charge and d is the mean cation–O distance. For $BaMoO_4$, $Z_i = 2$ and Ba–O ∼ 2.73 Å, giving tetrahedral bulk modulus of ∼60 GPa, close to our observed values.

Therefore, as in other scheelite compounds [9, 15], the compressibility in the scheelite phase may primarily be due to the larger and softer Ba–O bonds rather than W–O tetrahedral bonds.

To evaluate the space group of the second high pressure phase (phase III), we used the software DICVOL91 linked in the CRYSFIRE suite [34]. Seven non-overlapping diffraction lines of the high pressure phase were indexed to the monoclinic cells. The unit cells, as given by the CRYSFIRE suite, were refined for the best space group (i.e. missing reflections) with the help of Checkcell software [35]. This analysis gave a monoclinic cell (in $P2/c$ space group) having a figure of merit $M(7) = 46$. Final cell parameters determined with the help of Le Bail analysis of the observed diffraction pattern are $a = 6.396 \pm 0.002$ Å, $b = 6.727 \pm 0.001$ Å, $c = 3.098 \pm 0.001$ Å, and $\beta = 100.176° \pm 0.074$ (figure 8), with the goodness of fit parameters as $R_{wp} = 7\%$, $R_p = 4\%$.

In addition, we also carried out the further analyses with several competing monoclinic structures ($LaTaO_4(P2_1/c, Z = 4)$, $BaMnF_4$ ($Cmc2_1, Z = 4$) [36] and also the recently proposed $Cmca$ structure ($Z = 8$)). For this the transformed unit cell dimensions and the atomic coordinates were generated from the fergusonite phase for $P2_1/c$, and $Cmca$ space groups with the help of the Powdercell software [33]. The cell parameters of these space groups obtained from the Le Bail fits (shown in figure 8) are $P2_1/c$ ($a = 7.093 \pm 0.001$ Å, $b = 13.457 \pm 0.002$ Å, $c = 3.167 \pm 0.001$ Å, and $\gamma = 116.426° \pm 0.082$; $R_{wp} = 3\%$, $R_p = 2\%$), $Cmca$ ($a = 6.346 \pm 0.002$ Å, $b = 13.449 \pm 0.005$ Å, and $c = 3.059 \pm 0.002$Å; $R_{wp} = 9\%$, $R_p = 5\%$), $Cmc2_1$ ($a = 6.286 \pm 0.002$ Å, $b = 13.448 \pm 0.005$ Å, and $c = 3.174 \pm 0.002$ Å; $R_{wp} = 9\%$, $R_p = 5\%$). Though the Le Bail fits with $P2/c$ and $P2_1/c$ suggest the space group of the second high pressure phase to be either of these, detailed analyses based on FOX [37] and Rietveld refinement indicate that none of these structures are compatible with the observed diffraction pattern.

4. Conclusions

To conclude, our x-ray diffraction and Raman studies on barium molybdate show that it transforms to the fergusonite phase ∼5.8 GPa, as also observed in iso-structural barium tungstate and calcium tungstate. Beyond 7.2 GPa, the fergusonite phase transforms to another phase, the structure of which is yet unknown. On release of pressure from 15.8 GPa, this compound reverts back to the initial scheelite phase. Our results suggest that, in spite of different alkaline earth cations in the scheelite structured alkaline earth tungstates and molybdates, these may favourably transform to the fergusonite structure before transforming to a different lower symmetry phase.

References

[1] Ishii M and Kobayashi M 1991 *Prog. Cryst. Growth Charact.* **23** 245
[2] Faure N, Borel C, Couchaud M, Basset G, Templier R and Wyon C 1996 *Appl. Phys.* B **63** 593
[3] Angloher G, Bucci C, Cozzini C, von Feilitzsch F, Frank T, Hauff D, Henry S, Jagemann Th, Jochum J, Kraus H, Majorovits B, Ninkovie J, Petricca F, Pröbst F, Ramachers Y, Rau W, Seidel W, Stark M, Uchaikin S, Stodolsky L and Wulandari H 2004 *Nucl. Instrum. Methods Phys. Res.* A **520** 108
[4] Basiev T T, Sobol A A, Voronko K Yu and Zverev G G 2000 *Opt. Mater.* **15** 205
[5] David W I F, Glazer A M and Hewat A W 1979 *Phase Transit.* **1** 155
[6] Sarantopoulou E, Raptis Y S, Zouboulis E and Raptis C 1999 *Phys. Rev.* B **59** 4154
[7] Grzechnik A, Syassen K, Loa I, Hanfland M and Gesland J Y 2002 *Phys. Rev.* B **65** 104102
[8] Shieh S R, Ming L C and Jayaraman A 1996 *J. Phys. Chem. Solids* **57** 205
[9] Panchal V, Garg N, Chauhan A K, Sangeeta and Sharma S M 2004 *Solid State Commun.* **130** 203
[10] Christofilos D, Papagelis K, Ves S, Kourouklis G A and Raptis C 2002 *J. Phys.: Condens. Matter* **14** 12641
[11] Christofilos D, Kourouklis G A and Ves S 1995 *J. Phys. Chem. Solids* **56** 1125

[12] Jayaraman A, Batlogg B and Van Uitert L G 1983 *Phys. Rev.* B **28** 4774
[13] Jayaraman A, Wang S Y and Sharma S K 1995 *Phys. Rev.* B **52** 9886
[14] Sleight A W 1972 *Acta Crystallogr.* B **28** 2899
[15] Hazen R M, Finger L W and Mariathasan J W E 1985 *J. Phys. Chem. Solids* **46** 253
[16] Grzechnik A, Friese K, Dmitriev V, Weber H, Gesland J Y and Crichton W 2005 *J. Phys.: Condens. Matter* **17** 763
[17] Errandonea D, Somayazulu M and Häusermann D 2003 *Phys. Status Solidi* b **235** 162
[18] Grzechnik A, Crichton W A, Hanfland M and Van Smaalen S 2003 *J. Phys.: Condens. Matter* **15** 7261
[19] Errandonea D, Pellicer-Porres J, Manjon F J, Segura A, Ferrer-Roca Ch, Kumar R S, Tschauner O, Rodriguez-Hernandez P, Lopez-solano J, Radescu S, Mujica A, Munoz A and Aquilanti G 2005 *Phys. Rev.* B **72** 174106
[20] Grzechnik A, Crichton W A and Hanfland M 2005 *Phys. Status Solidi* b **242** 2795
[21] Crichton W A and Grzechnik A 2004 *Z. Kristallogr. NCS* **219** 337
[22] Grzechnik A, Crichton W A, Bouvier P, Dmitriev V, Weber H P and Gesland J Y 2004 *J. Phys.: Condens. Matter* **16** 7779
[23] Sharma S M and Sikka S K 1996 *Prog. Mater. Sci.* **40** 1
[24] Li S, Ahuja R and Johansson B 2004 *J. Phys.: Condens. Matter* **16** S983
[25] Christofilos D, Arvanitidis J, Kampasakali E, Papagelis K, Ves S and Kourouklis G A 2004 *Phys. Status Solidi* b **241** 3155
[26] Hammersely A P, Svensson S O, Hanfland M, Fitch A N and Hausermann D 1996 *High Pressure Res.* **14** 235
[27] Larson A C and von Dreele R B 2000 *GSAS: General Structure Analysis System* Los Alamos National Laboratory
[28] Mao H K, Xu J and Bell P M 1986 *J. Geophys. Res.* **91** 4673
[29] Dewaele A, Loubeyre P and Mezouar M 2004 *Phys. Rev.* B **70** 094112
[30] Liegeois-Duyckaerts M and Tarte P 1972 *Spectrochim. Acta* A **28** 2037
[31] Christofilos D, Ves S and Kourouklis G A 1996 *Phys. Status Solidi* b **198** 539
[32] Jayaraman A, Batlogg B and VanUitert L G 1985 *Phys. Rev.* B **31** 5423
[33] Kraus W and Nolze G 1998 *CPD Newsletter no. 20* International Union of Crystallography
[34] Shirley R 2002 *The Crysfire (2002) System for Automatic Powder Indexing: User's Manual* (Guildford: The Lattice Press)
[35] Laugier J and Bochu B http://www.inpg.fr/LMPG
[36] Keve E T, Abrahams S C and Bernstein J L 1969 *J. Chem. Phys.* **51** 4928
[37] Fox, Free Objects for Crystallography http://objcryst.sourceforge.net